Two-Dimensional Frequency-Domain Blind System Identification Using Higher Order Statistics with Application to Texture Synthesis

Chong-Yung Chi, *Senior Member, IEEE,* and Chii-Horng Chen

***Abstract*—In this paper, Shalvi and Weinstein's super-exponential (SE) algorithm using higher order statistics for blind deconvolution of one-dimensional (1-D) linear time-invariant systems is extended to a two-dimensional (2-D) SE algorithm. Then, a 2-D frequency-domain blind system identification (BSI) algorithm for 2-D linear shift-invariant (LSI) systems using the computationally efficient 2-D SE algorithm and the 2-D linear prediction error filter is proposed. In addition to the LSI system estimate, the proposed BSI algorithm also provides a minimum mean square error (MMSE) equalizer estimate and an MMSE signal enhancement filter estimate. Then, a texture synthesis method (TSM) using the proposed BSI algorithm is presented. Some simulation results to support the efficacy of the proposed BSI algorithm and some experimental results to support the efficacy of the proposed TSM are presented. Finally, some conclusions are drawn.**

***Index Terms*—Higher order statistics and texture synthesis, 2-D blind system identification, 2-D super-exponential algorithm.**

I. Introduction

ESTIMATION of a two-dimensional (2-D) linear shift-invariant (LSI) system $h[n_1, n_2]$ with only a given 2-D system output random field $y[n_1, n_2]$ is a blind system identification (BSI) problem that is essential in a variety of 2-D statistical signal processing applications, such as 2-D spectral estimation, texture image synthesis, classification, and image restoration [1]–[9], [11]–[16]. Parametric models, such as autoregressive (AR), moving average (MA), and autoregressive moving average (ARMA) models, have been widely used for $h[n_1, n_2]$, and thus, the BSI becomes a parameter estimation problem that often leads to mathematically tractable solutions with predictable performance [1]–[8], [11]–[15]. There have been a number of second-order statistics (SOS)-based algorithms reported for the estimation of parameters of $h[n_1, n_2]$, such as linear prediction based methods [1]–[3], least-squares (LS) solution based methods [4]–[6], and maximum-likelihood (ML) methods [5], [7]–[9]. In [4]–[6], 2-D AR parameters are estimated by the LS solution of a set of linear equations formed from autocorrelations (SOS) of $y[n_1, n_2]$. Assuming that $y[n_1, n_2]$ is Gaussian, Kashyap and Chellappa [5] and Sharma and Chellappa [7] estimate AR parameters using an ML estimator. Takelp *et al.* [8] proposed an image restoration method using an ARMA model for which the AR and MA parts correspond to the image model and the blur system, respectively. They estimate the ARMA parameters by also using an ML estimator with the assumption that the driving input of the image model is white Gaussian. Eom [9] uses a one-dimensional (1-D) function as an approximation to a 2-D MA model. The 1-D function is estimated also using an ML algorithm with the assumption that the 2-D spectrum of $y[n_1, n_2]$ is independent identically distributed (i.i.d.) complex Gaussian. Then, the 2-D MA model obtained from the estimated 1-D function is applied to synthesis of texture images. Due to the fact that SOS are blind to the system phase, only the magnitude information of 2-D LSI systems can be extracted by the SOS-based approaches mentioned above.

Higher order statistics (HOS), known as cumulants [10], which include both magnitude and phase information of non-Gaussian random fields, have been used for the estimation of 2-D AR or ARMA models that can be nonminimum-phase, asymmetric, and noncausal [11]–[16]. Bhattacharya *et al.* [11] estimate AR parameters by the LS solution of a set of linear equations formed from third-order cumulants of the given 2-D random field $y[n_1, n_2]$. Swami and Mendel [12] also estimate AR parameters by the LS solution of a set of linear equations formed from higher order (≥ 3) cumulants of $y[n_1, n_2]$. Then, MA parameters are estimated via a closed-form solution using cumulants of the residual signal obtained by removing the AR part from $y[n_1, n_2]$. Inverse filter criteria [13], [14] have been reported for estimating ARMA parameters. Tugnait [13] proposed three inverse filter criteria for jointly estimating AR and MA parameters, whereas only the estimated AR parameters are used for texture synthesis. Hall and Giannakis [14] proposed two inverse filter criteria for estimating AR parameters, whereras MA parameters are estimated either by a closed-form solution using higher order cumulants or by cumulant matching. Then, the estimated AR parameters are used for texture synthesis and classification. Hall and Giannakis [15] also estimate ARMA parameters by polyspectral matching, whereas only AR parameters are used for texture synthesis. On the other hand, Tsatsanis and Giannakis [16] proposed a nonparametric cumulant matching method for texture image classification. The computational load of the preceding HOS-based methods increases rapidly with the assumed model order, especially for those methods that find the

Manuscript received November 15, 1999; revised December 27, 2000. This work was supported by the National Science Council under Grants NSC 88-2218-E007-019 and NSC 89-2213-E-007-073. Part of this work was presented at the IEEE Workshop on Signal Processing Systems, Taipei, Taiwan R.O.C., October 20–22, 1999. The associate editor coordinating the review of this paper and approving it for publication was Prof. Dr. Ir. Bart L. R. De Moor.

The authors are with the Department of Electrical Engineering and Institute of Communications Engineering, National Tsing Hua University, Hsinchu, Taiwan, R.O.C. (e-mail: cychi@ee.nthu.edu.tw).

Publisher Item Identifier S 1053-587X(01)02249-8.

optimum model parameters through iterative nonlinear search procedure such as the aforementioned inverse filter criteria.

Shalvi and Weinstein [17], [18] proposed a family of blind deconvolution criteria to obtain the optimum 1-D inverse filter (linear equalizer) $v[n]$ using two cumulants of the inverse filter output signal with two different cumulant orders. It has been shown [17] that under the two assumptions [a1) signal-to-noise ratio (SNR) is infinite and a2) the linear time-invariant (LTI) channel $h[n]$ is stable and its inverse filter $h_{\rm INV}[n]$ exists], the optimum inverse filter $v[n]$ is a zero forcing (ZF) equalizer (i.e., $v[n] = \alpha h_{\rm INV}[n-\tau]$). However, one has to resort to iterative nonlinear optimization algorithms to find the optimum $v[n]$. Recently, Feng and Chi [19]–[21] reported performance analyses for the optimum inverse filter $v[n]$ associated with Shalvi and Weinstein's blind deconvolution criteria for finite SNR. The optimum inverse filter $v[n]$ possesses three properties [19]–[21] for finite SNR, including a relation between the minimum mean square error (MMSE) equalizer and the optimum $v[n]$, the stability property, and perfect phase equalization property. Based on the three properties of the optimum $v[n]$, Chi and Feng [22] proposed a blind channel estimation (BCE) algorithm, and meanwhile, the MMSE equalizer and MMSE signal enhancement filter can be readily estimated from the obtained channel estimate $\hat{h}[n]$.

Shalvi and Weinstein [23] also proposed an iterative super-exponential (SE) algorithm using higher order cumulants for 1-D blind channel equalization. At each iteration, the SE algorithm finds the 1-D inverse filter $v[n]$ by solving a set of linear equations formed from autocorrelations of measurements and higher order cross-cumulants between the equalized signal and measurements. Under the assumptions a1) and a2) mentioned above, the computationally efficient 1-D SE algorithm converges at a super-exponential rate, and the resultant $v[n]$ turns out to be a ZF equalizer.

In this paper, Shalvi and Weinstein's 1-D SE algorithm [23] is extended to the 2-D SE algorithm for blind deconvolution of 2-D LSI systems. Then, a computationally efficient 2-D frequency-domain BSI algorithm is proposed for estimating the unknown LSI system $h[n_1, n_2]$ using the well-known 2-D linear prediction error (LPE) filter and the inverse filter $v[n_1, n_2]$ obtained by the computationally efficient 2-D SE algorithm. The proposed 2-D BSI algorithm is robust against Gaussian noise, and the obtained system estimate $\hat{h}[n_1, n_2]$ is applied to texture synthesis.

The paper is organized as follows. Section II presents the 2-D SE algorithm for 2-D blind deconvolution of 2-D LSI systems needed by the proposed 2-D BSI algorithm that is presented in Section III. Then, a texture synthesis method (TSM) using the proposed 2-D BSI algorithm is presented in Section IV. Some simulation results to support the efficacy of the proposed BSI algorithm and some experimental results to support the efficacy of the proposed TSM are presented in Section V. Finally, we draw some conclusions.

II. Two-Dimensional Super-Exponential Algorithm

For ease of later use, let $\text{cum}\{s_1, s_2, \cdots, s_M\}$ denote the joint cumulant of random variables $s_1, s_2, \cdots, s_M$ [10] and

$$\text{cum}\{s: p, \cdots\} = \text{cum}\{\underbrace{s, \cdots, s}_{p \text{ terms}}, \cdots\}. \tag{1}$$

Assume that we are given a set of $N \times N$ measurements $y[n_1, n_2]$ modeled as

$$y[n_1, n_2] = x[n_1, n_2] + w[n_1, n_2] \tag{2}$$

where $x[n_1, n_2]$ is the noise-free output signal of an LSI system $h[n_1, n_2]$ driven by an unknown input signal $u[n_1, n_2]$, i.e.,

$$\begin{aligned} x[n_1, n_2] &= u[n_1, n_2] * h[n_1, n_2] \\ &= \sum_{k_1=-\infty}^{\infty} \sum_{k_2=-\infty}^{\infty} h[k_1, k_2] u[n_1 - k_1, n_2 - k_2] \end{aligned} \tag{3}$$

and $w[n_1, n_2]$ is additive measurement noise. Let us make the following assumptions about $u[n_1, n_2]$, $h[n_1, n_2]$, and $w[n_1, n_2]$, respectively.

A1) $u[n_1, n_2]$ is stationary complex, zero-mean, i.i.d., non-Gaussian with variance σ_u^2 and nonzero $(l+m)$th-order cumulant

$$\mu_{l,m} = \text{cum}\{u[n_1, n_2]: l, u^*[n_1, n_2]: m\} \tag{4}$$

where l and m are non-negative integers, $(l+m) \geq 3$, and the superscript $*$ denotes complex conjugation.

A2) Both $h[n_1, n_2]$ and its inverse system $h_{\rm INV}[n_1, n_2]$ are stable LSI systems.

A3) $w[n_1, n_2]$ is stationary complex, zero-mean, colored Gaussian with variance σ_w^2 given by

$$w[n_1, n_2] = \eta[n_1, n_2] * b[n_1, n_2] \tag{5}$$

where $\eta[n_1, n_2]$ is complex zero-mean white Gaussian with variance σ_η^2, and $b[n_1, n_2]$ is a stable LSI system. Moreover, $w[n_1, n_2]$ is statistically independent of $u[n_1, n_2]$.

Note that $w[n_1, n_2]$ is white Gaussian when $b[n_1, n_2]$ is an all-pass system and that $y[n_1, n_2]$ is also a stationary non-Gaussian random field with correlation function

$$\begin{aligned} r_{yy}[k_1, k_2] &= E\{y[n_1, n_2] y^*[n_1 - k_1, n_2 - k_2]\} \\ &= \sigma_u^2 h[n_1, n_2] * h^*[-n_1, -n_2] \\ &\quad + \sigma_\eta^2 b[n_1, n_2] * b^*[-n_1, -n_2] \end{aligned} \tag{6}$$

and continuous power spectrum (discrete-time Fourier transform of $r_{yy}[k_1, k_2]$)

$$\begin{aligned} S_{yy}(\omega_1, \omega_2) &= S_{xx}(\omega_1, \omega_2) + S_{ww}(\omega_1, \omega_2) \\ &= \sigma_u^2 |H(\omega_1, \omega_2)|^2 + \sigma_\eta^2 |B(\omega_1, \omega_2)|^2 \end{aligned} \tag{7}$$

where $H(\omega_1, \omega_2)$ and $B(\omega_1, \omega_2)$ are the frequency responses of the 2-D LSI systems $h[n_1, n_2]$ and $b[n_1, n_2]$, respectively. Next, let us briefly review Shalvi and Weinstein 1-D SE algorithm [21], [23] before presenting the proposed 2-D SE algorithm.

A. Review of the 1-D SE Algorithm

Assume that $y[n]$, $n = 0, 1, \cdots, N-1$ are the corresponding 1-D measurements modeled by (2). Let $v[n]$, $n = 0, \cdots, q_1$ be the 1-D causal inverse filter of order q_1 (q_1th-order causal FIR filter). The 1-D inverse filter output $e[n]$ is given by

$$\begin{aligned} e[n] &= v[n] * y[n] = \sum_{k=0}^{q_1} v[k] y[n-k] \\ &= \mathbf{v}^T \mathbf{y}[n] = u[n] * g[n] + w[n] * v[n] \end{aligned} \tag{8}$$

where $\mathrm{v} = (v[0], v[1], \cdots, v[q_1])^T$, $\mathrm{y}[n] = (y[n], y[n-1], \cdots, y[n-q_1])^T$, and

$$g[n] = h[n] * v[n] \tag{9}$$

is the overall system after deconvolution. The 1-D SE algorithm iteratively finds the inverse filter $v[n]$ by solving the following linear equations:

$$\sum_{k=0}^{q_1} v[k] E\{y[m] y^*[m+k-n]\} = \mathrm{cum}\{e[m]: p, e^*[m]: q, y^*[m-n]\}, \qquad n = 0, \cdots, q_1 \tag{10}$$

where p and q are non-negative integers, and $p+q \geq 2$. At the ith iteration, by expressing (10) in matrix form, the 1-D SE algorithm updates v with $\|\mathrm{v}\| = 1$ ($\mathcal{L}_2$ norm of v) via

$$\mathrm{v}_i = \frac{\mathcal{R}_y^{-1} \mathrm{d}_{ey}}{\|\mathcal{R}_y^{-1} \mathrm{d}_{ey}\|} \tag{11}$$

where $\mathcal{R}_y = E\{\mathrm{y}^*[n] \mathrm{y}^T[n]\}$ and

$$\mathrm{d}_{ey} = \mathrm{cum}\{e_{i-1}[n] : p\ , e_{i-1}^*[n]: q, \mathrm{y}^*[n]\}, \qquad p+q \geq 2 \tag{12}$$

in which $e_{i-1}[n] = y[n] * v_{i-1}[n]$ is the equalized signal obtained at the $(i-1)$th iteration, where $v_{i-1}[n]$ is the inverse filter associated with v_{i-1}.

As v_i converges, the associated $v_i[n]$ is the obtained 1-D inverse filter $v[n]$. It has been shown [23] that the amount of intersymbol interference $\mathrm{ISI}\{g_i[n] = h[n] * v_i[n]\}$ defined as [17], [23]

$$\mathrm{ISI}\{g[n]\} = \frac{\sum_n |g[n]|^2 - \max\{|g[n]|^2, \quad \forall n\}}{\max\{|g[n]|^2, \quad \forall n\}} \tag{13}$$

decreases to zero ($g_i[n] = \alpha \delta[n-\tau]$ for all $\alpha \neq 0$) at a super-exponential rate for $\mathrm{SNR} = \infty$ and q_1 sufficiently large.

B. Two-Dimensional SE Algorithm

Let $v[n_1, n_2]$ be the 2-D inverse filter with a truncated quarter plane (TQP) region of support given by [1], [2]

$$\Omega_{\mathrm{TQP}}[p_1, p_2] = \{[n_1, n_2]: n_1 = 0 \sim p_1, n_2 = 0 \sim p_2\}. \tag{14}$$

Let $y[n_1, n_2]$ input to the 2-D FIR filter $v[n_1, n_2]$ and $e[n_1, n_2]$ be the corresponding output signal, i.e.,

$$\begin{aligned} e[n_1, n_2] &= y[n_1, n_2] * v[n_1, n_2] \\ &= \sum_{k_1=0}^{p_1} \sum_{k_2=0}^{p_2} v[k_1, k_2] y[n_1 - k_1, n_2 - k_2] \\ &= u[n_1, n_2] * g[n_1, n_2] + w[n_1, n_2] * v[n_1, n_2] \end{aligned} \tag{15}$$

where

$$g[n_1, n_2] = h[n_1, n_2] * v[n_1, n_2] \tag{16}$$

is the 2-D overall system after deconvolution (equalization).

The 2-D SE algorithm, that is, a direct 2-D extension of the 1-D SE algorithm, iteratively finds the inverse filter $v[n_1, n_2]$ by solving the following linear equations:

$$\begin{aligned} &\sum_{k=0}^{p_1} \sum_{l=0}^{p_2} v[k, l] E\{y[m, n] y^*[m+k-n_1, n+l-n_2]\} \\ &\quad = \mathrm{cum}\{e[m, n]: p, e^*[m, n]: q, y^*[m-n_1, n-n_2]\} \\ &\qquad \forall [n_1, n_2] \in \Omega_{\mathrm{TQP}}[p_1, p_2] \end{aligned} \tag{17}$$

where p and q are non-negative integers, and $p+q \geq 2$.

Let $(n)_p$ denote "n modulo p," let $\lfloor k \rfloor$ denote the largest integer less than or equal to k, and let

$$\begin{aligned} \mathbf{v} = (&v[0, 0], v[1, 0], \cdots, v[p_1, 0], v[0, 1], v[1, 1], \\ &\cdots, v[p_1, 1], \cdots, v[p_1, p_2])^{\mathrm{T}} \end{aligned} \tag{18}$$

including the filter coefficients $v[n_1, n_2]$ for all $[n_1, n_2] \in \Omega_{\mathrm{TQP}}[p_1, p_2]$. At the ith iteration, by expressing (17) in a matrix form, the 2-D SE algorithm updates the unknown parameter vector $\mathbf{v}$ with $\|\mathbf{v}\| = 1$ via

$$\mathbf{v}_i = \frac{\mathbf{R}_y^{-1} \cdot \mathbf{d}_{ey}}{\|\mathbf{R}_y^{-1} \cdot \mathbf{d}_{ey}\|} \tag{19}$$

where $\mathbf{R}_y$ is a $[(p_1+1)(p_2+1)] \times [(p_1+1)(p_2+1)]$ autocorrelation matrix with the $[k, l]$th element given by

$$[\mathbf{R}_y]_{k,l} = E\left\{ y[n_1, n_2] y^* \left[n_1 + (k-1)_{p_1+1} - (l-1)_{p_1+1} \right. \right. \left. \left. n_2 + \left\lfloor \frac{k-1}{p_1+1} \right\rfloor - \left\lfloor \frac{l-1}{p_1+1} \right\rfloor \right] \right\} \tag{20}$$

and $\mathbf{d}_{ey}$ is a $(p_1+1)(p_2+1) \times 1$ vector with the kth element given by

$$[\mathbf{d}_{ey}]_k = \mathrm{cum}\left\{ e_{i-1}[n_1, n_2]: p, e_{i-1}^*[n_1, n_2]: q, \right. \left. y^* \left[n_1 - (k-1)_{p_1+1}, n_2 - \left\lfloor \frac{k-1}{p_1+1} \right\rfloor \right] \right\} \tag{21}$$

where $e_{i-1}[n_1, n_2]$ is the equalized signal obtained at the $(i-1)$th iteration, i.e.,

$$e_{i-1}[n_1, n_2] = y[n_1, n_2] * v_{i-1}[n_1, n_2] \tag{22}$$

in which $v_{i-1}[n_1, n_2]$ is the 2-D inverse filter associated with $\mathbf{v}_{i-1}$.

As $\mathbf{v}_i$ converges, the associated $v_i[n_1, n_2]$ is the obtained 2-D inverse filter $v[n_1, n_2]$. As the 1-D SE algorithm, it can also be shown that $\mathrm{ISI}\{g_i[n_1, n_2] = h[n_1, n_2] * v_i[n_1, n_2]\}$ [which is the 2-D counterpart of $\mathrm{ISI}\{g_i[n]\}$ given by (13)] decreases to zero ($g_i[n_1, n_2] = \alpha \delta[n_1 - \tau_1, n_2 - \tau_2]$ for all $\alpha \neq 0$) at a super-exponential rate for $\mathrm{SNR} = \infty$ and p_1 and p_2 sufficiently large. That is, the obtained inverse filter $v[n_1, n_2] = \alpha h_{\mathrm{INV}}[n_1 - \tau_1, n_2 - \tau_2]$ is a 2-D ZF equalizer. However, when the SNR is finite, the obtained $v[n_1, n_2]$ can be shown to possess the following two properties as p_1 and p_2 are sufficiently large.

P1) The inverse filter $V(\omega_1, \omega_2)$ (2-D discrete-time Fourier transform of $v[n_1, n_2]$) is related to the

2-D MMSE equalizer [24], which is denoted by $V_{\rm MSE}(\omega_1, \omega_2)$, via

$$V(\omega_1, \omega_2) = \alpha \cdot D(\omega_1, \omega_2) V_{\rm MSE}(\omega_1, \omega_2) \tag{23}$$

where α is a nonzero constant

$$V_{\rm MSE}(\omega_1, \omega_2) = \frac{\sigma_u^2 \cdot H^*(\omega_1, \omega_2)}{S_{yy}(\omega_1, \omega_2)} = \frac{\sigma_u^2 \cdot H^*(\omega_1, \omega_2)}{\sigma_u^2 |H(\omega_1, \omega_2)|^2 + \sigma_\eta^2 |B(\omega_1, \omega_2)|^2} \tag{24}$$

and $D(\omega_1, \omega_2)$ is the 2-D discrete-time Fourier transform of the 2-D sequence $d[n_1, n_2]$, which is given by

$$d[n_1, n_2] = (g[n_1, n_2])^p (g^*[n_1, n_2])^q \tag{25}$$

where $g[n_1, n_2]$ is given by (16).

P2) For the case of complex $y[n_1, n_2]$ and $p = q + 1$, the phase response $\arg[V(\omega_1, \omega_2)]$ is related to the system phase $\arg[H(\omega_1, \omega_2)]$ by

$$\arg[V(\omega_1, \omega_2)] = -\arg[H(\omega_1, \omega_2)] - \omega_1 \tau_1 - \omega_2 \tau_2 + \kappa \tag{26}$$

where τ_1 and τ_2 are unknown integers, and κ is an unknown constant. On the other hand, for the case of real $y[n_1, n_2]$, (26) is also true with $\kappa = 0$, as $p + q$ is odd.

The proofs of P1) and P2) are given in Appendices A and B, respectively.

We remark that the 2-D (1-D) SE algorithm is also applicable when the given measurements $y[n_1, n_2]$ ($y[n]$) are real, and it is the same for all $p \geq 0$, $q \geq 0$, and $(p + q) \geq 2$, and surely, the obtained 2-D inverse filter $v[n_1, n_2]$ ($v[n]$) is real as well. Let us conclude this section with the following two remarks regarding the 2-D SE algorithm.

R1) By P2), the resultant overall system $G(\omega_1, \omega_2) = H(\omega_1, \omega_2) V(\omega_1, \omega_2)$ can be a zero-phase system (i.e., $g[n_1, n_2] = g^*[-n_1, -n_2]$) if the 2-D space shift $[\tau_1, \tau_2]$ and constant phase shift κ can be compensated. Moreover, it can be easily shown from (25) that when $g[n_1, n_2]$ is zero phase, $d[n_1, n_2]$ is also zero phase (i.e., $d[n_1, n_2] = d^*[-n_1, -n_2]$).

R2) The property P2) also implies that a space shift $[k_1, k_2]$ and a complex scale factor $e^{j\phi}$ may exist between $v_i[n_1, n_2]$ and $v_{i-1}[n_1, n_2]$. However, the 2-D space shift $[k_1, k_2]$ between $v_i[n_1, n_2]$ and $v_{i-1}[n_1, n_2]$ is always equal to $[0, 0]$ because the location $[m_1, m_2]$ for which $|g_i[m_1, m_2]| = \max\{|g_i[n_1, n_2]|, \forall [n_1, n_2]\}$ is always invariant for all i as SNR $= \infty$ [23]. Therefore, the following convergence rule for the 2-D SE algorithm is suggested:

$$\min_{\phi} \left\{ \left\| \mathbf{v}_i - e^{j\phi} \mathbf{v}_{i-1} \right\|^2 \right\} = 2 - 2 \cdot |\mathbf{v}_i^H \mathbf{v}_{i-1}| < \epsilon_{\rm SE} \tag{27}$$

where $\mathbf{v}_i^H$ is the complex conjugate of the transpose of $\mathbf{v}_i$, and $\epsilon_{\rm SE} > 0$ is the assigned convergence tolerance. On the other hand, an initial condition $v_0[n_1, n_2]$ is needed to initialize the 2-D SE algorithm. By our experience, $v_0[n_1, n_2] = \delta[n_1 - l_1, n_2 - l_2]$ is a good choice, where $[l_1, l_2]$ is in the proximity of the center of $\Omega_{\rm TQP}[p_1, p_2]$ because most energy of $v_i[n_1, n_2]$ can rapidly spread over $\Omega_{\rm TQP}[p_1, p_2]$, and thus, $v_i[n_1, n_2]$ approaches the resultant $v[n_1, n_2]$ in a more efficient manner.

III. Two-Dimensional Blind System Identification Algorithm

First of all, let us briefly review the 2-D LPE filter that is widely used in statistical signal processing, which, together with the inverse filter $v[n_1, n_2]$ obtained by the 2-D SE algorithm, is needed by the 2-D BSI algorithm for the magnitude estimation of the 2-D LSI system $h[n_1, n_2]$. Let $a[n_1, n_2]$ be a 2-D LPE filter associated with measurements $y[n_1, n_2]$ with leading coefficient $a[0, 0] = 1$ and a truncated nonsymmetric half plane (TNSHP) region of support given by [1], [2]

$$\Omega_{\rm TNSHP}[p_1, p_2] = \{[n_1, n_2]: n_1 = 1 \sim p_1, n_2 = -p_2 \sim p_2\} \cup \{[n_1, n_2]: n_1 = 0, n_2 = 0 \sim p_2\}. \tag{28}$$

The prediction error, which is denoted by $\varepsilon[n_1, n_2]$, is the output signal of the 2-D LPE filter driven by $y[n_1, n_2]$, i.e.,

$$\varepsilon[n_1, n_2] = y[n_1, n_2] * a[n_1, n_2] = \sum_{[k_1, k_2] \in \Omega_{\rm TNSHP}[p_1, p_2]} \sum a[k_1, k_2] y[n_1 - k_1, n_2 - k_2]. \tag{29}$$

The optimum LPE filter coefficients $a[n_1, n_2]$ for all $[n_1, n_2] \in \Omega_{\rm TNSHP}[p_1, p_2]$, except $a[0, 0] = 1$ by minimizing $E\{|\varepsilon[n_1, n_2]|^2\}$, can be obtained by solving the following 2-D Yule–Walker (linear) equations [1], [2]

$$\sum_{[k_1, k_2] \in \Omega_{\rm TNSHP}[p_1, p_2]} \sum a[k_1, k_2] \cdot E\{y[k_1, k_2] y^*[k_1 - n_1, k_2 - n_2]\} = 0, \quad \forall [n_1, n_2] (\neq [0, 0]) \in \Omega_{\rm TNSHP}[p_1, p_2]. \tag{30}$$

Moreover, for sufficiently large p_1 and p_2, $a[n_1, n_2]$ performs as a whitening filter or an amplitude equalizer, i.e.,

$$|A(\omega_1, \omega_2)|^2 \propto \frac{1}{S_{yy}(\omega_1, \omega_2)} = \frac{1}{\sigma_u^2 |H(\omega_1, \omega_2)|^2 + \sigma_\eta^2 |B(\omega_1, \omega_2)|^2} \quad \text{[by (7)]}. \tag{31}$$

As a remark, $\Omega_{\rm TQP}[p_1, p_2]$ given by (14) rather than $\Omega_{\rm TNSHP}[p_1, p_2]$ given by (28) can also be used as the region of support of the 2-D LPE filter, as long as the resultant $S_{\varepsilon\varepsilon}(\omega_1, \omega_2)$ is flat.

From (23), (24), and (31), it can be easily shown that

$$|H(\omega_1, \omega_2)| = \beta \cdot \frac{\Gamma(\omega_1, \omega_2)}{|D(\omega_1, \omega_2)|} \tag{32}$$

where β is a positive constant, and

$$\Gamma(\omega_1, \omega_2) = \frac{|V(\omega_1, \omega_2)|}{|A(\omega_1, \omega_2)|^2}. \tag{33}$$

Based on (32) and P2) for the magnitude estimation and phase estimation of $h[n_1, n_2]$, respectively, the following 2-D FFT-based frequency-domain BSI algorithm is proposed.

A. Two-Dimensional BSI Algorithm

Step 1) Blind deconvolution.

T1) With finite data $y[n_1, n_2]$, obtain the inverse filter $v[n_1, n_2]$ using the 2-D SE algorithm presented in Section II and the 2-D LPE filter $a[n_1, n_2]$ using the 2-D Yule–Walker equations given by (33).

T2) Compute $V(\omega_{k_1}, \omega_{k_2})$, $A(\omega_{k_1}, \omega_{k_2})$, and $\Gamma(\omega_{k_1}, \omega_{k_2})$ given by (30) using the $(L \times L)$-point 2-D FFT, where $\omega_{k_1} = 2\pi k_1/L$ and $\omega_{k_2} = 2\pi k_2/L$, $k_1 = 0, 1, \cdots, L-1$, $k_2 = 0, 1, \cdots, L-1$.

Step 2) Magnitude estimation.

S1) Set $i = 0$. Set initial values $|H^{[0]}(\omega_{k_1}, \omega_{k_2})|$ for $|H(\omega_{k_1}, \omega_{k_2})|$ and a convergence tolerance $\epsilon_H > 0$.

S2) Set $i = i + 1$. Compute

$$G^{[i-1]}(\omega_{k_1}, \omega_{k_2}) = \left|H^{[i-1]}(\omega_{k_1}, \omega_{k_2})\right| \cdot |V(\omega_{k_1}, \omega_{k_2})|$$

and its $(L \times L)$-point 2-D IFFT $g^{[i-1]}[n_1, n_2]$.

S3) Compute $d[n_1, n_2]$ using (25) with $g[n_1, n_2] = g^{[i-1]}[n_1, n_2]$ and its $(L \times L)$-point 2-D FFT $D(\omega_{k_1}, \omega_{k_2})$.

S4) Compute

$$\left|\tilde{H}(\omega_{k_1}, \omega_{k_2})\right| = \frac{\Gamma(\omega_{k_1}, \omega_{k_2})}{|D(\omega_{k_1}, \omega_{k_2})|} \tag{34}$$

by (32), and then, $|H^{[i]}(\omega_{k_1}, \omega_{k_2})|$ is obtained as $|\tilde{H}(\omega_{k_1}, \omega_{k_2})|$ normalized by $\sum_{k_1=0}^{L-1}\sum_{k_2=0}^{L-1} |\tilde{H}(\omega_{k_1}, \omega_{k_2})|^2 = 1$.

S5) If

$$\sum_{k_1=0}^{L-1}\sum_{k_2=0}^{L-1}\left[\left|H^{[i]}(\omega_{k_1}, \omega_{k_2})\right| - \left|H^{[i-1]}(\omega_{k_1}, \omega_{k_2})\right|\right]^2 > \epsilon_H$$

then go to S2).

Step 3) Estimation of $H(\omega_1, \omega_2)$.

With the system magnitude estimate $|\hat{H}(\omega_{k_1}, \omega_{k_2})| = |H^{[i]}(\omega_{k_1}, \omega_{k_2})|$ obtained in Step 2) and the phase estimate $\arg[\hat{H}(\omega_{k_1}, \omega_{k_2})] = -\arg[V(\omega_{k_1}, \omega_{k_2})]$ [by P2)] obtained in Step 1), $\hat{H}(\omega_{k_1}, \omega_{k_2})$, $k_1 = 0, 1, \cdots, L-1$, $k_2 = 0, 1, \cdots, L-1$ are obtained as

$$\hat{H}(\omega_{k_1}, \omega_{k_2}) = \left|H^{[i]}(\omega_{k_1}, \omega_{k_2})\right| \cdot \exp\{-j \arg[V(\omega_{k_1}, \omega_{k_2})]\} \tag{35}$$

and the associated estimate $\hat{h}[n_1, n_2]$ is the $(L \times L)$-point 2-D IFFT of $\hat{H}(\omega_{k_1}, \omega_{k_2})$.

Three worthy remarks regarding the proposed BSI algorithm are as follows.

R3) The proposed 2-D BSI algorithm is a frequency-domain estimation algorithm that provides estimates $\hat{H}(\omega_{k_1} = 2\pi k_1/L, \omega_{k_2} = 2\pi k_2/L)$, $k_1 = 0, 1, \cdots, L-1$, $k_2 = 0, 1, \cdots, L-1$ with the given non-Gaussian (real or complex) measurements $y[n_1, n_2]$. When measurements $y[n_1, n_2]$ are real, the LPE filter $a[n_1, n_2]$ and the inverse filter $v[n_1, n_2]$ in T1) of Step 1 are also real; as mentioned in Section II, the latter obtained by the 2-D SE algorithm is the same for all $p \geq 0$, $q \geq 0$ and odd $p + q$ (≥ 3). On the other hand, the region of support associated with the estimate $\hat{h}[n_1, n_2]$ can be arbitrary as long as the 2-D FFT size $L \times L$ is chosen sufficiently large so that aliasing effects on the resultant $\hat{h}[n_1, n_2]$ are negligible.

R4) The obtained estimate $\hat{H}(\omega_1, \omega_2)$ is robust against Gaussian noise because (32), on which the magnitude estimation is based, and P2), on which the phase estimation is based, are true, regardless of the value of σ_η^2 (or the value of SNR), although magnitude responses of the inverse filter $v[n_1, n_2]$ and the 2-D LPE filter $a[n_1, n_2]$ obtained in Step 1 depend on SNR.

R5) Assume that $\lambda[n_1, n_2]$ is the inverse filter obtained by processing the 2-D LPE filter output signal $\varepsilon[n_1, n_2]$ [see (29)] with the 2-D SE algorithm. Then, the inverse filter $V(\omega_1, \omega_2)$ in Step 1 can also be obtained by

$$V(\omega_1, \omega_2) = \Lambda(\omega_1, \omega_2) \cdot A(\omega_1, \omega_2). \tag{36}$$

We empirically found that the 2-D SE algorithm always converges faster by processing $\varepsilon[n_1, n_2]$ than by processing $y[n_1, n_2]$ when the dynamic range of $S_{yy}(\omega_1, \omega_2)$ is large. The reasons for this are as follows. By (2), (3) and (29), the signal $\varepsilon[n_1, n_2]$ can be expressed as

$$\begin{aligned}\varepsilon[n_1, n_2] = {} & u[n_1, n_2] * (h[n_1, n_2] * a[n_1, n_2]) \\ & + w[n_1, n_2] * a[n_1, n_2].\end{aligned} \tag{37}$$

As mentioned above, the 2-D LPE filter basically performs as an amplitude equalizer that significantly removes the system magnitude distortion leading to $S_{\varepsilon\varepsilon}(\omega_1, \omega_2)$ much flatter than $S_{yy}(\omega_1, \omega_2)$. In other words, the dynamic range of the former is much smaller than that of the latter, and the associated 2-D LSI system $h[n_1, n_2] * a[n_1, n_2]$ is typically closer to an allpass system (a phase-distortion system) to be equalized by the 2-D SE algorithm than $h[n_1, n_2]$. On the other hand, the iterative procedure in Step 2 for magnitude estimation converges fast, regardless of whether or not the preprocessing of the LPE filter is involved by our experience.

With the 2-D LSI system estimate $\hat{H}(\omega_1, \omega_2)$ obtained by the proposed BSI algorithm, an MMSE equalizer $V_{\mathrm{MSE}}(\omega_1, \omega_2)$ and an MMSE signal enhancement filter, which is denoted by $\mathcal{H}(\omega_1, \omega_2)$, can be estimated from $\hat{H}(\omega_1, \omega_2)$ and the 2-D LPE filter $A(\omega_1, \omega_2)$. The MMSE equalizer $V_{\mathrm{MSE}}(\omega_1, \omega_2)$ for estimating $u[n_1, n_2]$ can be estimated as

$$\hat{V}_{\mathrm{MSE}}(\omega_1, \omega_2) = \frac{\hat{H}^*(\omega_1, \omega_2)}{\hat{S}_{yy}(\omega_1, \omega_2)} \quad \text{[by (24)]} \tag{38}$$

$$= \hat{H}^*(\omega_1, \omega_2)|A(\omega_1, \omega_2)|^2 \quad \text{[by (31)]} \tag{39}$$

up to a scale factor and a space shift.

It is known that the noncausal zero-phase MMSE signal enhancement filter for estimating the noise-free signal $x[n_1, n_2]$ is given by [24]

$$\begin{aligned}\mathcal{H}(\omega_1, \omega_2) &= \frac{S_{xx}(\omega_1, \omega_2)}{S_{yy}(\omega_1, \omega_2)} = \frac{\sigma_u^2 |H(\omega_1, \omega_2)|^2}{S_{yy}(\omega_1, \omega_2)} \\ &= V_{\mathrm{MSE}}(\omega_1, \omega_2) H(\omega_1, \omega_2) \quad \text{[by (24)]}\end{aligned} \tag{40}$$

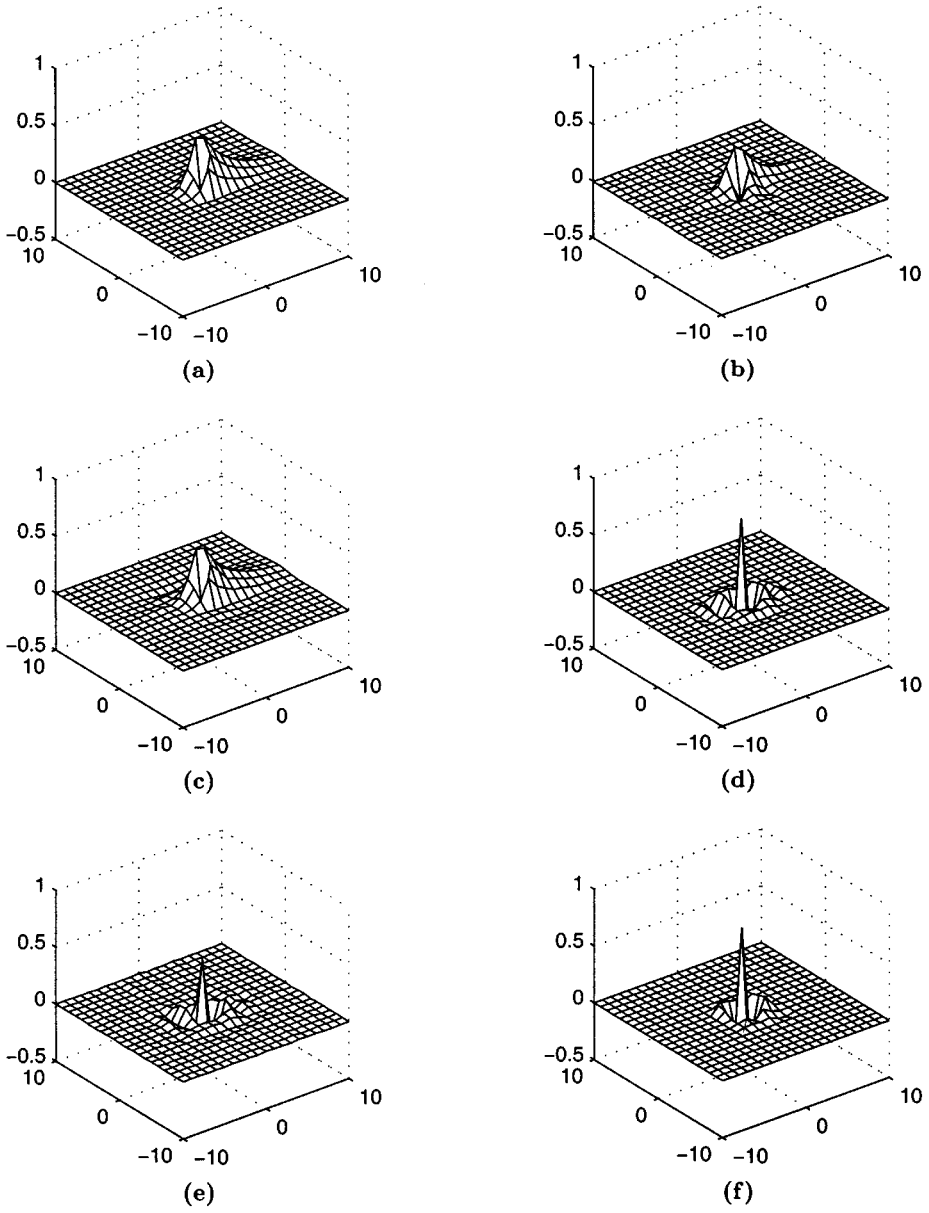

Fig. 1. Simulation results of Example 1 for $N \times N = 256 \times 256$ and SNR = 5 dB (lowpass Gaussian noise). (a) True system $h[n_1, n_2]$. (b) and (c) Average $\overline{h}[n_1, n_2]$ associated with Tugnait's method and the proposed BSI algorithm, respectively. (d) True $v_{\mathrm{MSE}}[n_1, n_2]$. (e) and (f) Average $\overline{v}_{\mathrm{MSE}}[n_1, n_2]$ associated with Tugnait's method and the proposed BSI algorithm, respectively.

which leads to the MMSE signal enhancement filter estimate given by (up to a scale factor)

$$\hat{\mathcal{H}}(\omega_1, \omega_2) = \frac{\hat{S}_{xx}(\omega_1,\omega_2)}{\hat{S}_{yy}(\omega_1,\omega_2)} \tag{41}$$

$$= \hat{V}_{\mathrm{MSE}}(\omega_1, \omega_2) \cdot \hat{H}(\omega_1, \omega_2) \quad \text{[by (40)]}. \tag{42}$$

One can also obtain different MMSE equalizer estimates and MMSE signal enhancement filter estimates using (38) and (41), respectively, with $\hat{S}_{yy}(\omega_1, \omega_2)$ obtained by different 2-D power spectral estimation methods such as the 2-D averaged periodogram [1].

IV. TSM

Assume that we are given a noise-free real texture image $\tilde{x}[n_1, n_2]$ (finite gray levels) and that $y[n_1, n_2]$ is the mean removed version of $\tilde{x}[n_1, n_2]$. The proposed TSM includes the following four steps:

Step 1) Obtain the texture image model $\hat{h}[n_1, n_2]$ and the 2-D LPE filter $A(\omega_1, \omega_2)$ associated with $y[n_1, n_2]$ using the proposed 2-D BSI algorithm.

Step 2) Obtain the MMSE equalizer estimate $\hat{V}_{\mathrm{MSE}}(\omega_1, \omega_2)$ using (39), and then, obtain the MMSE estimate of the driving input $u[n_1, n_2]$ by

$$\hat{u}_{\mathrm{MSE}}[n_1, n_2] = y[n_1, n_2] * \hat{v}_{\mathrm{MSE}}[n_1, n_2]. \tag{43}$$

Step 3) Generate a random field $\tilde{u}[n_1, n_2]$ that has the same histogram as $\hat{u}_{\mathrm{MSE}}[n_1, n_2]$. Then, obtain a zero-mean synthetic texture image by

$$\tilde{y}[n_1, n_2] = \tilde{u}[n_1, n_2] * \gamma \hat{h}[n_1, n_2] \tag{44}$$

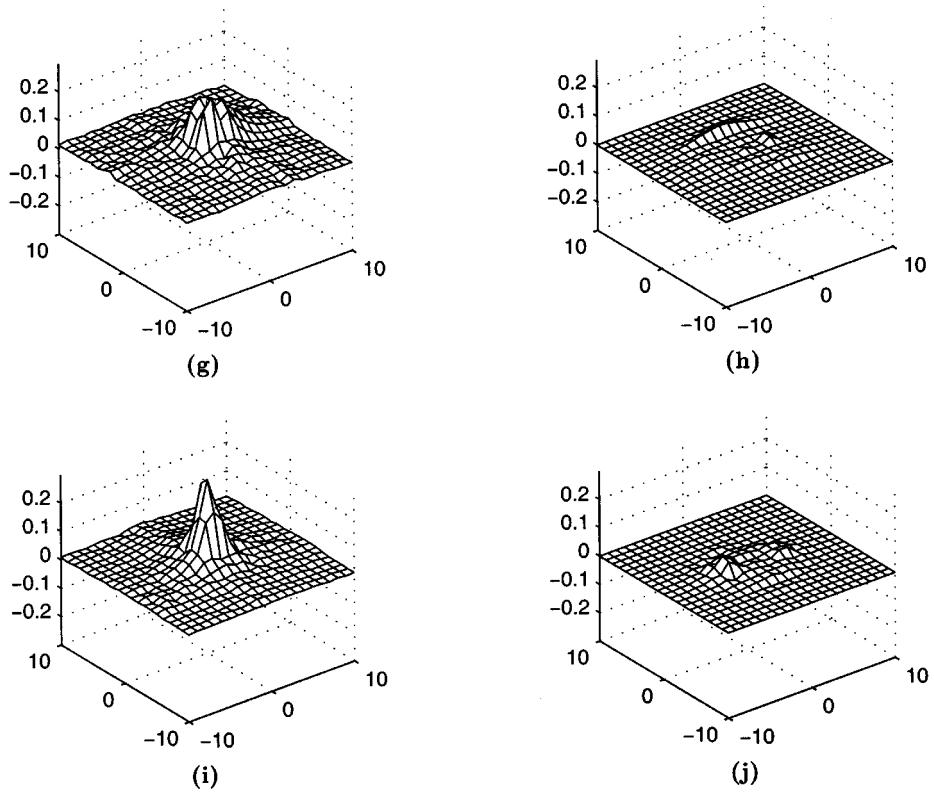

Fig. 1. *(Continued.)* Simulation results of Example 1 for $N \times N = 256 \times 256$ and SNR = 5 dB (lowpass Gaussian noise). (g) and (h) RMS error $\rho_{\rm h}[n_1, n_2]$ associated with Tugnait's method and the proposed BSI algorithm, respectively. (i) and (j) RMS error $\rho_{\rm MSE}[n_1, n_2]$ associated with Tugnait's method and the proposed BSI algorithm, respectively.

where the scale factor γ is chosen such that $E\{|\tilde{y}[n_1, n_2]|^2\} = E\{|y[n_1, n_2]|^2\}$.

Step 4) Obtain the synthetic texture image $\hat{\tilde{x}}[n_1, n_2]$ by adding $E\{\tilde{x}[n_1, n_2]\}$ to $\tilde{y}[n_1, n_2]$.

Note that the scale factor γ in Step 3 is chosen such that the synthetic texture image $\hat{\tilde{x}}[n_1, n_2]$ and the original texture image $\tilde{x}[n_1, n_2]$ have the same variance due to the noise-free assumption for $\tilde{x}[n_1, n_2]$. Let us conclude this section with the following remark.

R6) The proposed TSM basically follows the texture synthesis procedure reported in [6] and [13]–[15], except that the MMSE equalizer estimate $\hat{V}_{\rm MSE}(\omega_1, \omega_2)$ instead of the ZF equalizer estimate $\hat{V}_{\rm ZF}(\omega_1, \omega_2) = 1/\hat{H}(\omega_1, \omega_2)$ is used in Step 2. The MMSE equalizer estimate is preferable to the ZF equalizer estimate because the latter may enhance the noise due to modeling error in practical applications, although they are the same for the noise-free case [24].

V. Simulation and Experimental Results

In this section, some simulation results are presented to support that the proposed 2-D BSI algorithm is effective, and some experimental results are presented to support the efficacy of the proposed TSM. In both the simulation and the experiment, the synthetic measurements $y[n_1, n_2]$ and the texture images used were real, and the parameters used by the proposed 2-D BSI algorithm were as follows. In Step 1, the 2-D SE algorithm was employed to find the real 2-D inverse filter $v[n_1, n_2]$ with $p + q = 3$ and $\epsilon_{\rm SE} = 10^{-3}$. In Step 2, $|H^{[0]}(\omega_{k_1}, \omega_{k_2})| = 1$ for all k_1 and k_2, FFT size $L \times L = 32 \times 32$ in the simulation, $L \times L = 256 \times 256$ in the experiment, and $\epsilon_H = 10^{-5}$ were used.

For comparison, the results obtained using Tugnait's method [13] that maximizes the following inverse filter criterion

$$J_{4,2}(\boldsymbol{\theta}) = \frac{|\text{cum}\{e[n_1, n_2]: 4\}|}{|E\{e^2[n_1, n_2]\}|^2} \tag{45}$$

are also presented, where the parameter vector $\boldsymbol{\theta}$ includes AR and MA parameters of the unknown 2-D LSI system. The iterative Fletcher–Powell algorithm [25] was used to obtain the optimum $\boldsymbol{\theta}$. To initialize the Fletcher–Powell algorithm, the initial condition for $\boldsymbol{\theta}$ was set to true model parameters in the simulation. In the experiment, a 5×5 nonsymmetric AR model with region of support $\Omega[2, 2]$ [see (B.1) in Appendix B] was assumed , and the initial condition for $\boldsymbol{\theta}$ was obtained by Kashyap and Chellappa's approximate ML (AML) approach [5] (which yields symmetric AR parameters). Next, let us present the simulation results.

A. Simulation Results

Two simulation examples are to be presented only for $\hat{H}(\omega_1, \omega_2)$ given by (35) and $\hat{V}_{\rm MSE}(\omega_1, \omega_2)$ given by (39) because the MMSE signal enhancement filter estimate $\hat{\mathcal{H}}(\omega_1, \omega_2)$ given by (42) will become redundant. In the simulation, the driving input signal $u[n_1, n_2]$ was assumed to be a real zero-mean, exponentially distributed, i.i.d., random field with variance $\sigma_u^2 = 1$ that was convolved with the chosen 2-D LSI

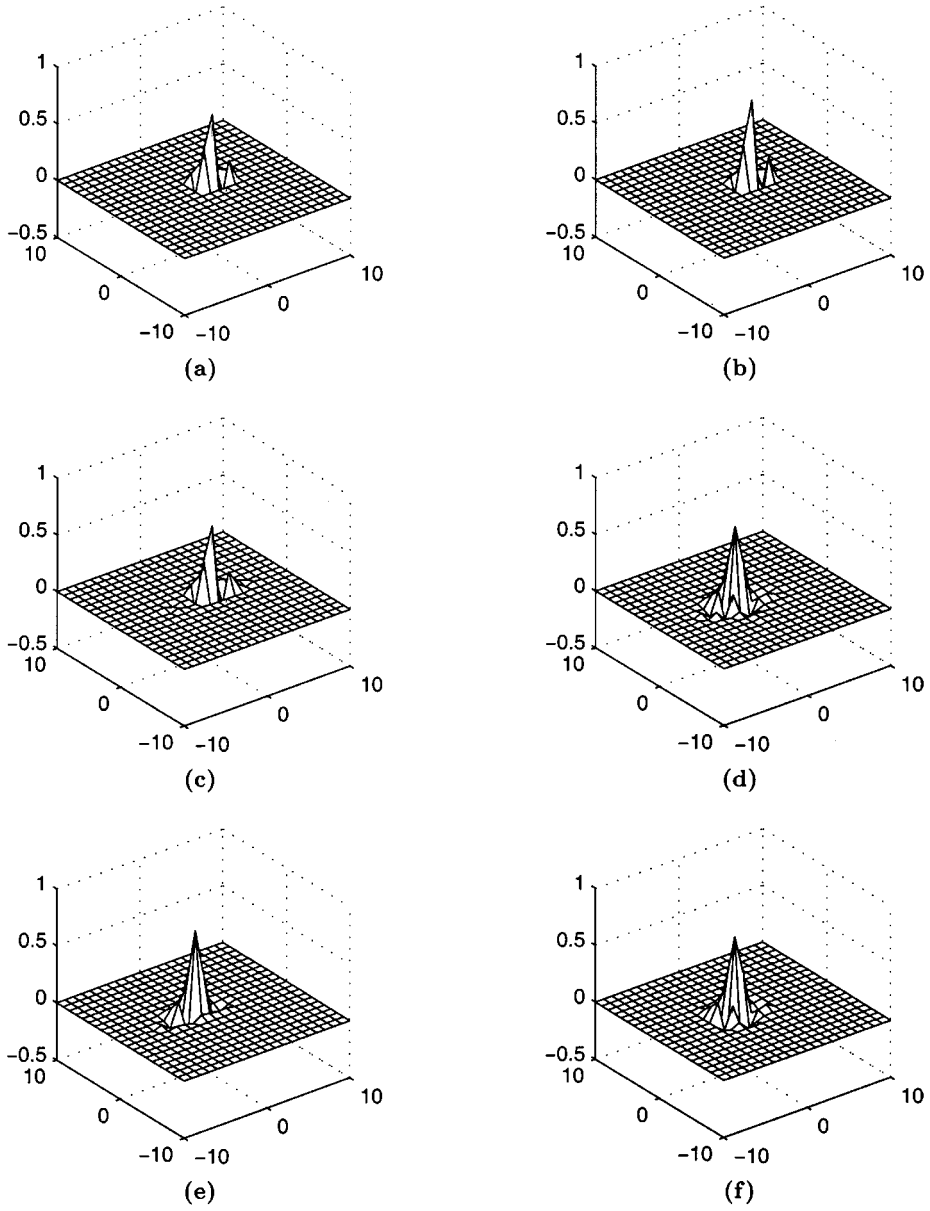

Fig. 2. Simulation results of Example 2 for $N \times N = 256 \times 256$ and SNR = 5 dB (white Gaussian noise). (a) True system $h[n_1, n_2]$. (b) and (c) Average $\overline{h}[n_1, n_2]$ associated with Tugnait's method and the proposed BSI algorithm, respectively. (d) True $v_{\rm MSE}[n_1, n_2]$. (e) and (f) Average $\overline{v}_{\rm MSE}[n_1, n_2]$ associated with Tugnait's method and the proposed BSI algorithm, respectively.

system $h[n_1, n_2]$ to generate the noise-free synthetic $N \times N$ data $x[n_1, n_2]$. Then, the synthetic $y[n_1, n_2]$ was obtained by adding a real white or colored Gaussian noise $w[n_1, n_2]$ to $x[n_1, n_2]$. Then, each of the proposed 2-D BSI algorithm and Tugnait's method was employed to process $y[n_1, n_2]$ to obtain an estimate $\hat{H}(\omega_1, \omega_2)$ from which (39) and the associated estimate $\hat{V}_{\rm MSE}(\omega_1, \omega_2)$ was obtained.

Thirty independent runs were performed for each of the two examples. Let $\hat{h}_i[n_1, n_2]$ and $\hat{v}_{{\rm MSE},i}[n_1, n_2]$ denote the obtained estimates $\hat{h}[n_1, n_2]$ and $\hat{v}_{\rm MSE}[n_1, n_2]$ normalized by unit energy at the ith run, respectively. The 2-D space shift between $\hat{h}_i[n_1, n_2]$ and the true $h[n_1, n_2]$ and that between $\hat{v}_{{\rm MSE},i}[n_1, n_2]$ and the true $v_{\rm MSE}[n_1, n_2]$ were artificially removed. Then, the average $\overline{h}[n_1, n_2]$ of the obtained 30 estimates $\hat{h}_i[n_1, n_2]$ and the associated root mean square (RMS) error $\rho_{\rm h}[n_1, n_2]$ were calculated with the true $h[n_1, n_2]$ normalized by unit energy prior to computing $\rho_{\rm h}[n_1, n_2]$. In the same fashion, the average $\overline{v}_{\rm MSE}[n_1, n_2]$ and the associated RMS error $\rho_{\rm MSE}[n_1, n_2]$ were also calculated from the obtained 30 estimates $\hat{v}_{{\rm MSE},i}[n_1, n_2]$. Next, let us turn to Example 1.

Example 1—ARMA Model: In this example, the unknown 2-D LSI system $h[n_1, n_2]$ used was a 2-D ARMA model with a 3×3 nonsymmetric support taken from [13] as follows:

$$\begin{aligned} x[n_1, n_2] &- 0.004x[n_1+1, n_2+1] + 0.0407x[n_1+1, n_2] \\ &- 0.027x[n_1+1, n_2-1] - 0.2497x[n_1, n_2+1] \\ &- 0.568x[n_1, n_2-1] + 0.1037x[n_1-1, n_2+1] \\ &- 0.3328x[n_1-1, n_2] + 0.1483x[n_1-1, n_2-1] \\ &= u[n_1, n_2] - 0.5u[n_1+1, n_2] - 0.5u[n_1, n_2+1] \\ &- u[n_1, n_2-1] - u[n_1-1, n_2]. \end{aligned} \tag{46}$$

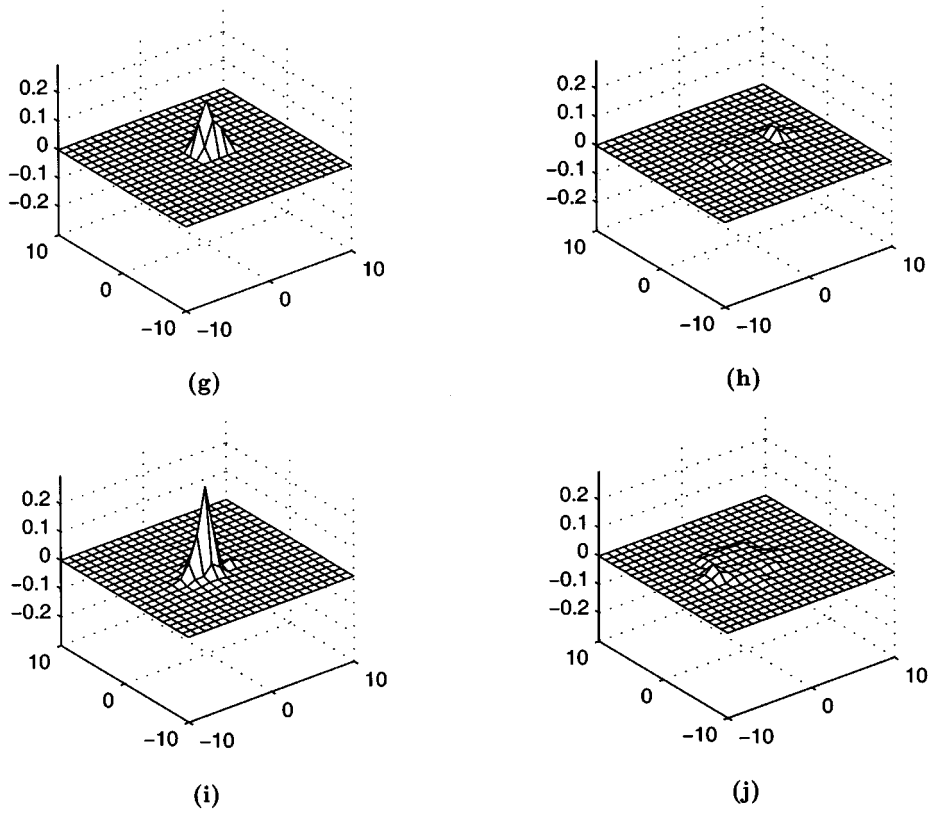

Fig. 2. *(Continued.)* Simulation results of Example 2 for $N \times N = 256 \times 256$ and SNR = 5 dB (white Gaussian noise). (g) and (h) RMS error $\rho_{\rm h}[n_1, n_2]$ associated with Tugnait's method and the proposed BSI algorithm, respectively. (i) and (j) RMS error $\rho_{\rm MSE}[n_1, n_2]$ associated with Tugnait's method and the proposed BSI algorithm, respectively.

In each run, a 256×256 synthetic $y[n_1, n_2]$ was generated for SNR $= \sigma_x^2/\sigma_w^2 = 5$ dB and $w[n_1, n_2]$ assumed to be real low-pass Gaussian with $B(z_1, z_2) = (1+0.8z_1^{-1})\cdot(1+0.8z_2^{-1})$ [see (5)]. In Step 1 of the proposed 2-D BSI algorithm, the region of support for the 2-D LPE filter $a[n_1, n_2]$ was $\Omega_{\rm TNSHP}[5, 5]$, and the 2-D SE algorithm was employed with the initial condition $v_0[n_1, n_2] = \delta[n_1 - 2, n_2 - 2]$ and the region of support $\Omega_{\rm TQP}[5, 5]$ for the 2-D inverse filter $v[n_1, n_2]$.

The proposed BSI algorithm spent only three iterations for magnitude estimation (see Step 2) at each run. Fig. 1(a) and (d) show the true $h[n_1, n_2]$ and $v_{\rm MSE}[n_1, n_2]$, respectively. Fig. 1(b), (e), (g), and (i) show the obtained $\overline{h}[n_1, n_2]$, $\overline{v}_{\rm MSE}[n_1, n_2]$, $\rho_{\rm h}[n_1, n_2]$, and $\rho_{\rm MSE}[n_1, n_2]$, respectively, associated with Tugnait's method. Fig. 1(c), (f), (h) and (j) show the corresponding results associated with the proposed BSI algorithm. One can see from these figures that $\overline{h}[n_1, n_2]$ and $\overline{v}_{\rm MSE}[n_1, n_2]$ shown in Fig. 1(c) and (f) associated with the proposed BSI algorithm are quite close to the true $h[n_1, n_2]$ and $v_{\rm MSE}[n_1, n_2]$, which are shown in Fig. 1(a) and (d), respectively. Meanwhile, the associated $\rho_{\rm h}[n_1, n_2]$ and $\rho_{\rm MSE}[n_1, n_2]$ shown in Fig. 1(h) and (j) are also small. Values of $\rho_{\rm h}[n_1, n_2]$ and $\rho_{\rm MSE}[n_1, n_2]$ associated with the proposed BSI algorithm are considerably smaller than those associated with Tugnait's method. These simulation results indicate that the proposed 2-D BSI algorithm outperforms Tugnait's method for the case of the ARMA system and low SNR (5 dB).

Example 2—MA Model: In this example, $h[n_1, n_2]$ used was a 2-D MA(2,3) model taken from [26] as follows:

$$\begin{aligned} x[n_1, n_2] = {} & u[n_1, n_2] - 0.8u[n_1 - 1, n_2] + 0.2u[n_1 - 2, n_2] \\ & + 1.8u[n_1, n_2 - 1] - 1.44u[n_1 - 1, n_2 - 1] \\ & + 0.36u[n_1 - 2, n_2 - 1] - 0.5u[n_1, n_2 - 2] \\ & + 0.4u[n_1 - 1, n_2 - 2] - 0.1u[n_1 - 2, n_2 - 2] \\ & + 0.5u[n_1, n_2 - 3] - 0.4u[n_1 - 1, n_2 - 3] \\ & + 0.1u[n_1 - 2, n_2 - 3]. \end{aligned} \tag{47}$$

In each run, a 256×256 synthetic $y[n_1, n_2]$ was generated for SNR = 5 dB and $w[n_1, n_2]$ assumed to be real white Gaussian. In Step 1) of the proposed 2-D BSI algorithm, the region of support for $a[n_1, n_2]$ and $v[n_1, n_2]$ and initial condition $v_0[n_1, n_2]$ were the same as those used in Example 1.

The proposed BSI algorithm spent only three iterations for magnitude estimation in obtaining one estimate $\hat{h}[n_1, n_2]$ and four iterations in obtaining the other 29. Fig. 2(a)–(j) show the simulation results corresponding to those shown in Fig. 1(a)–(j), respectively. Again, one can also see from these figures that the obtained $\overline{h}[n_1, n_2]$ and $\overline{v}_{\rm MSE}[n_1, n_2]$ associated with the proposed BSI algorithm are good approximations of $h[n_1, n_2]$ and $v_{\rm MSE}[n_1, n_2]$, respectively. Meanwhile, the associated $\rho_{\rm h}[n_1, n_2]$ and $\rho_{\rm MSE}[n_1, n_2]$ shown in Fig. 2(h) and (j) are also small. Values of $\rho_{\rm h}[n_1, n_2]$ and $\rho_{\rm MSE}[n_1, n_2]$ associated with the proposed BSI algorithm are also considerably smaller than those associated with Tugnait's method. These simulation results also indicate that the proposed 2-D BSI algorithm outperforms Tugnait's method for this case of MA system and low SNR (5 dB).

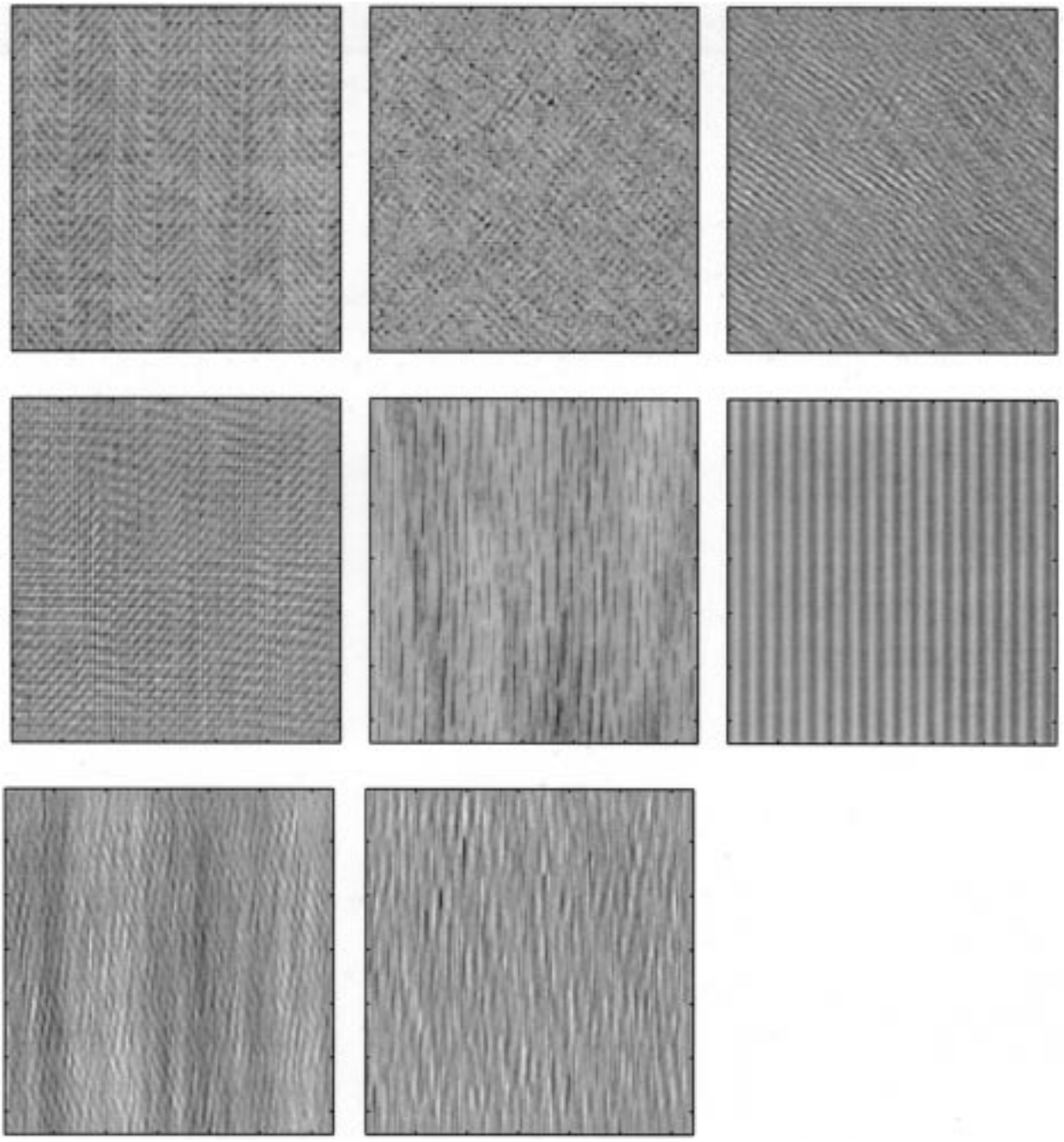

Fig. 3. Experimental results of Example 3. Windows (1,1) and (2,2) original herringbone weave and wood images, respectively; windows (1,2) and (2,3) synthetic herringbone weave and wood images obtained using Kashyap and Chellappa's AML algorithm with symmetric 5×5 AR model, respectively; windows (1,3) and (3,1) synthetic herringbone weave and wood images obtained using Tugnait's method with nonsymmetric 5×5 AR model, respectively; windows (2,1) and (3,2) synthetic herringbone weave and wood images obtained using the proposed TSM, respectively.

B. Experimental Results

Recall that the proposed 2-D BSI algorithm is needed by the proposed TSM. In Step 1 of the proposed 2-D BSI algorithm, the region of support for the 2-D LPE filter $a[n_1, n_2]$ was $\Omega_{\mathrm{TNSHP}}[5, 5]$ in the experiment, whereas the 2-D SE algorithm was employed with $v_0[n_1, n_2] = \delta[n_1 - 3, n_2 - 3]$ and the region of support $\Omega_{\mathrm{TQP}}[6, 6]$ for the 2-D inverse filter $v[n_1, n_2]$.

Example 3—Texture Synthesis: Four 128×128 texture images, herringbone weave, wood, raffia, and sand taken from University of Southern California—Signal and Image Processing Institute (USC-SIPI) Image Data Base were used for texture synthesis using the proposed TSM. The proposed BSI algorithm spent 12, four, four, and four iterations for magnitude estimation (Step 2) in obtaining $\hat{H}(\omega_1, \omega_2)$ associated with herringbone weave, wood, raffia, and sand images, respectively. The experimental results are shown in Figs. 3 and 4. Windows (1,1), (2,2) in Fig. 3 and those in Fig. 4 show the original herringbone weave, wood, raffia, and sand images, respectively. Windows (1,2), (2,3) in Fig. 3 and those in Fig. 4 show the synthetic herringbone weave, wood, raffia, and sand images, respectively, associated with Kashyap and Chellappa's AML algorithm. Windows (1,3), (3,1) in Fig. 3 and those in Fig. 4 show the synthetic

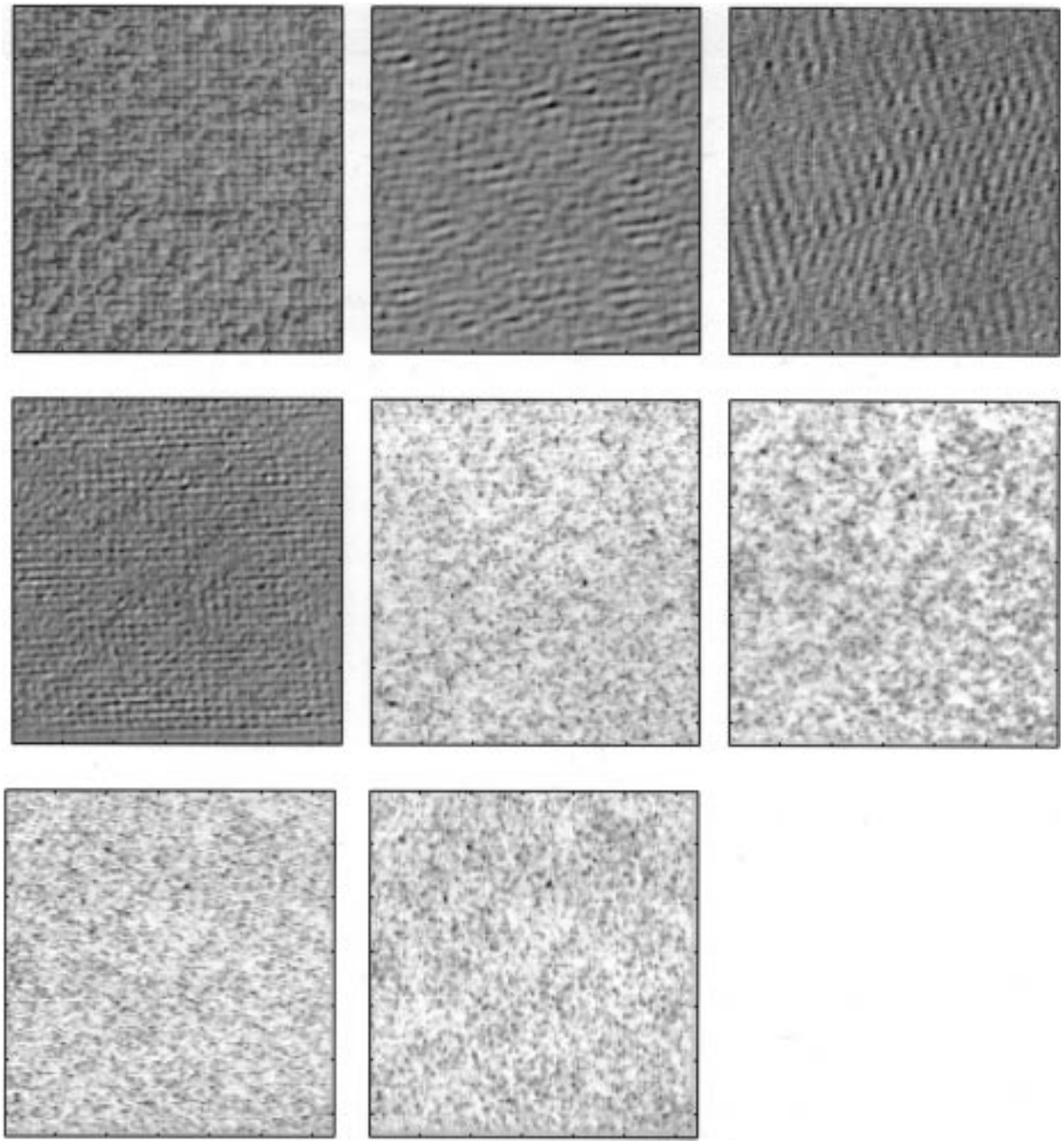

Fig. 4. Experimental results of Example 3. Windows (1,1) and (2,2) original raffia and sand images, respectively; windows (1,2) and (2,3) synthetic raffia and sand images obtained using Kashyap and Chellappa's AML algorithm with symmetric 5×5 AR model, respectively; windows (1,3) and (3,1) synthetic raffia and sand images obtained using Tugnait's method with nonsymmetric 5×5 AR model, respectively; windows (2,1) and (3,2) synthetic raffia and sand images obtained using the proposed TSM, respectively.

herringbone weave, wood, raffia, and sand images, respectively, associated with Tugnait's method. Windows (2,1), (3,2) in Fig. 3 and those in Fig. 4 show the synthetic herringbone weave, wood, raffia, and sand images, respectively, associated with the proposed TSM. From these figures, one can see that the four synthetic texture images associated with the proposed TSM quite resemble the four respective original texture images, and visually, they look more similar to the four respective original texture images than those associated with Kashyap and Chellappa's AML algorithm and Tugnait's method. These experimental results support the efficacy of the proposed TSM.

VI. Conclusions

A computationally efficient 2-D SE algorithm for blind deconvolution of 2-D LSI systems with only a given non-Gaussian random field has been presented that is a direct extension of Shalvi and Weinsetin's 1-D SE algorithm for blind equalization of LTI systems. Then, a 2-D BSI algorithm for the estimation of an arbitrary 2-D LSI system $h[n_1, n_2]$ using the 2-D LPE filter $a[n_1, n_2]$ and the inverse filter $v[n_1, n_2]$ obtained by the proposed 2-D SE algorithm, which is an FFT-based frequency-domain estimation algorithm, was presented. Step 2 of

the proposed 2-D BSI algorithm itself is an iterative algorithm for system magnitude estimation that always converges fast by our experience. However, its convergence analysis is needed and left for future research. After $H(\omega_1, \omega_2)$ is estimated by the proposed 2-D BSI algorithm, an MMSE equalizer estimate $\hat{V}_{\mathrm{MSE}}(\omega_1, \omega_2)$ and an MMSE signal enhancement filter estimate $\hat{\mathcal{H}}(\omega_1, \omega_2)$ can be obtained by (39) and (42), respectively. Moreover, a TSM using the proposed BSI algorithm was presented. Then, some simulation results were provided to support the good performance of the proposed 2-D BSI algorithm even for low SNR (5 dB). Some experimental results were also provided to support that the proposed TSM is effective. Let us emphasize that the proposed TSM is merely one of texture synthesis methods with the LSI model for texture images, whereas the nonlinear model can also be used for texture images such as [27]. Other applications of the proposed 2-D BSI algorithm such as image enhancement and restoration, texture image classification, and 2-D spectral estimation are left to future research.

APPENDIX A
PROOF OF P1)

Because ISI$\{\alpha g[n_1-\tau_1, n_2-\tau_2]\}$ is invariant for all $\alpha \neq 0$, τ_1, and τ_2, the assumption of $p_1 \to \infty$ and $p_2 \to \infty$ (sufficiently large) for $0 \ll \tau_1 \ll p_1$ and $0 \ll \tau_2 \ll p_2$ is equivalent to the assumption that the region of support associated with $v[n_1, n_2]$ is doubly infinite for $\tau_1 = \tau_2 = 0$. With this equivalent assumption, the linear equations given by (17) can be rewritten as follows:

$$\begin{aligned}
&\sum_{k=-\infty}^{\infty}\sum_{l=-\infty}^{\infty} v[k, l]E\{y[m, n]y^*[m+k-n_1, n+l-n_2]\} \\
&\quad = \sum_{k=-\infty}^{\infty}\sum_{l=-\infty}^{\infty} v[k, l]r_{yy}[n_1-k, n_2-l] \\
&\quad = \mathrm{cum}\{e[m, n]\colon p, e^*[m, n]\colon q, y^*[m-n_1, n-n_2]\} \\
&\qquad \forall [n_1, n_2]. \qquad \text{(A.1)}
\end{aligned}$$

First of all, let us simplify the higher order cross-cumulant cum$\{e[m, n]\colon p, e^*[m, n]\colon q, y^*[m-n_1, n-n_2]\}$ on the right side of (A.1) as follows:

$$\begin{aligned}
&\mathrm{cum}\{e[m, n]\colon p, e^*[m, n]\colon q, y^*[m-n_1, n-n_2]\} \\
&\quad = \mathrm{cum}\left\{e[m, n]\colon p, e^*[m, n]\colon q \right. \\
&\qquad \left. \sum_{k_1=-\infty}^{\infty}\sum_{k_2=-\infty}^{\infty} u^*[k_1, k_2] \cdot h^*[m-n_1-k_1, n-n_2-k_2]\right\} \\
&\quad = \sum_{k_1=-\infty}^{\infty}\sum_{k_2=-\infty}^{\infty} h^*[m-n_1-k_1, n-n_2-k_2] \\
&\qquad \cdot \mathrm{cum}\left\{\left(\sum_{i_1=-\infty}^{\infty}\sum_{i_2=-\infty}^{\infty} g[i_1, i_2]u[m-i_1, n-i_2]\right)\colon p, \right. \\
&\qquad \left. \left(\sum_{l_1=-\infty}^{\infty}\sum_{l_2=-\infty}^{\infty} g^*[l_1, l_2]u^*[m-l_1, n-l_2]\right)\colon q, \right. \\
&\qquad \left. u^*[k_1, k_2]\right\} \\
&\quad = \mu_{p, q+1}\sum_{k_1=-\infty}^{\infty}\sum_{k_2=-\infty}^{\infty} h^*[m-n_1-k_1, n-n_2-k_2] \\
&\qquad \cdot (g[m-k_1, n-k_2])^p(g^*[m-k_1, n-k_2])^q \quad \text{[by A1)]} \\
&\quad = \mu_{p, q+1}\sum_{k_1=-\infty}^{\infty}\sum_{k_2=-\infty}^{\infty} h^*[k_1-n_1, k_2-n_2] \\
&\qquad \cdot (g[k_1, k_2])^p(g^*[k_1, k_2])^q. \qquad \text{(A.2)}
\end{aligned}$$

In the derivation of (A.2), we have replaced $y[n_1, n_2]$ [see (2)] and $e[n_1, n_2]$ [see (15)] by $x[n_1, n_2]$ [see (3)] and $u[n_1, n_2] * g[n_1, n_2]$, respectively, because $w[n_1, n_2]$ is Gaussian with higher order ($\geq$3) cumulants equal to zero [10]. Substituting cum$\{e[m, n]\colon p, e^*[m, n]\colon q, y^*[m-n_1, n-n_2]\}$ given by (A.2) into (A.1) and then taking the 2-D discrete-time Fourier transform of both sides of the resultant equation with respect to $[n_1, n_2]$ yields

$$V(\omega_1, \omega_2)S_{yy}(\omega_1, \omega_2) = \mu_{p, q+1}H^*(\omega_1, \omega_2)D(\omega_1, \omega_2) \qquad \text{(A.3)}$$

where $D(\omega_1, \omega_2)$ is the 2-D discrete-time Fourier transform of the 2-D signal $d[n_1, n_2]$ given by (25). Further substituting $S_{yy}(\omega_1, \omega_2)$ given by (7) into (A.3), one can come up with

$$\begin{aligned}
V(\omega_1, \omega_2) &= \frac{\mu_{p,q+1}}{\sigma_u^2}\frac{\sigma_u^2 \cdot H^*(\omega_1, \omega_2)}{\sigma_u^2|H(\omega_1, \omega_2)|^2 + \sigma_\eta^2|B(\omega_1, \omega_2)|^2} \\
&\quad \cdot D(\omega_1, \omega_2) \\
&= \frac{\mu_{p,q+1}}{\sigma_u^2} \cdot D(\omega_1, \omega_2)V_{\mathrm{MSE}}(\omega_1, \omega_2) \qquad \text{(A.4)}
\end{aligned}$$

that is the same as (23) with $\alpha = \mu_{p, q+1}/\sigma_u^2$. Thus, we have completed the proof of P1).

APPENDIX B
PROOF OF P2)

Proving P2) is equivalent to proving that the overall system $G(\omega_1, \omega_2)$ is zero phase, assuming $\tau_1 = \tau_2 = \kappa = 0$ without loss of generality. The proof to be presented below needs the following two assumptions:

B1) $g[n_1, n_2] \neq 0$ only for $[n_1, n_2] \in \Omega[K, K]$ and $g[0, 0] > 0$, where

$$\Omega[p_1, p_2] = \{[n_1, n_2]\colon n_1 = -p_1 \sim p_1, n_2 = -p_2 \sim p_2\}. \qquad \text{(B.1)}$$

B2) $0 < |g[K, K]| < |g[n_1, n_2]|, \forall [n_1, n_2] \in \Omega[K, K]$, $[n_1, n_2] \neq [K, K]$, and $[n_1, n_2] \neq [-K, -K]$.

Let

$$\begin{aligned}
f[n_1, n_2] &= d[n_1, n_2] * g^*[-n_1, -n_2] \\
&= \sum_{m_1=-K}^{K}\sum_{m_2=-K}^{K}(g[m_1, m_2])^p(g^*[m_1, m_2])^q \\
&\quad \cdot g^*[m_1-n_1, m_2-n_2] \quad \text{[by B1)]} \qquad \text{(B.2)}
\end{aligned}$$

where $p \geq 0$, $q \geq 0$, and $(p+q) \geq 2$. It can be easily shown, from (23) and (24), that the 2-D discrete-time Fourier transform

$$F(\omega_1, \omega_2) = D(\omega_1, \omega_2)G^*(\omega_1, \omega_2) \geq 0 \tag{B.3}$$

which implies $f[n_1, n_2] = f^*[-n_1, -n_2]$ and $f[0, 0] \geq |f[n_1, n_2]|$. Note, from (B.2), that $f[n_1, n_2] \neq 0$ only for $[n_1, n_2] \in \Omega[2K, 2K]$ by B1). Next, let us consider the case of complex $g[n_1, n_2]$ followed by the case of real $g[n_1, n_2]$.

A. Complex $g[n_1, n_2]$ with $p = q + 1$

For $p = q + 1$, (B.2) can be rewritten as

$$f[n_1, n_2] = \sum_{m_1=-K}^{K} \sum_{m_2=-K}^{K} g[m_1, m_2]|g[m_1, m_2]|^{2q} \cdot g^*[m_1 - n_1, m_2 - n_2]. \tag{B.4}$$

It can be easily seen from (B.4) that

$$\begin{aligned} f[2K, 2K] &= |g[K, K]|^{2q} g[K, K]g^*[-K, -K] \\ &= f^*[-2K, -2K] \\ &= |g[-K, -K]|^{2q} g^*[-K, -K]g[K, K] \end{aligned} \tag{B.5}$$

which implies

$$|g[K, K]| = |g[-K, -K]|. \tag{B.6}$$

Again, by (B.4), simplifying $f[2K, 2K-1] = f^*[-2K, -2K+1]$ results in

$$\begin{aligned} &g[K, K]g^*[-K, -K+1] \\ &\quad \cdot \{|g[-K, -K+1]|^{2q} - |g[K, K]|^{2q}\} \\ &= g^*[-K, -K]g[K, K-1] \\ &\quad \cdot \{|g[K, K-1]|^{2q} - |g[-K, -K]|^{2q}\} \end{aligned} \tag{B.7}$$

which by B2) and (B.6) further gives rise to

$$|g[K, K-1]| = |g[-K, -K+1]|. \tag{B.8}$$

Moreover, it can be easily shown from (B.6)–(B.8) that

$$\frac{g[K, K]}{g^*[-K, -K]} = \frac{g[K, K-1]}{g^*[-K, -K+1]}. \tag{B.9}$$

Similarly, letting $f[n_1, n_2] = f^*[-n_1, -n_2]$ given by (B.4) for $n_1 = K+1, \cdots, 2K$, $n_2 = 0, \cdots, 2K$ and $n_1 = K$, $n_2 = K, \cdots, 2K$, one can end up with

$$|g[n_1, n_2]| = |g[-n_1, -n_2]|, \qquad \forall\, [n_1, n_2] \in \Omega[K, K] \tag{B.10}$$

and

$$\frac{g[n_1, n_2]}{g^*[-n_1, -n_2]} = \frac{g[0, 0]}{g^*[0, 0]} = 1, \qquad \forall\, [n_1, n_2] \in \Omega[K, K] \tag{B.11}$$

[since $g[0, 0] > 0$ by B1)] that implies

$$g[n_1, n_2] = g^*[-n_1, -n_2], \qquad \forall\, [n_1, n_2] \in \Omega[K, K]. \tag{B.12}$$

B. Real $g[n_1, n_2]$ with Odd $p + q$

For real $g[n_1, n_2]$, (B.2) can be rewritten as

$$f[n_1, n_2] = \sum_{m_1=-K}^{K} \sum_{m_2=-K}^{K} (g[m_1, m_2])^{p+q} g[m_1 - n_1, m_2 - n_2]. \tag{B.13}$$

It can be easily seen from (B.13) that

$$\begin{aligned} f[2K, 2K] &= (g[K, K])^{p+q} g[-K, -K] = f[-2K, -2K] \\ &= (g[-K, -K])^{p+q} g[K, K] \end{aligned} \tag{B.14}$$

which implies

$$|g[K, K]| = |g[-K, -K]|. \tag{B.15}$$

By (B.13) and $f[2K, 2K-1] = f[-2K, -2K+1]$, we have

$$\begin{aligned} &g[K, K]g[-K, -K+1] \\ &\quad \cdot \{(g[-K, -K+1])^{p+q-1} - (g[K, K])^{p+q-1}\} \\ &= g[-K, -K]g[K, K-1] \\ &\quad \cdot \{(g[K, K-1])^{p+q-1} - (g[-K, -K])^{p+q-1}\} \end{aligned} \tag{B.16}$$

which, by B2) and (B.15), further gives rise to

$$|g[K, K-1]| = |g[-K, -K+1]| \tag{B.17}$$

and

$$\frac{g[K, K]}{g[-K, -K]} = \frac{g[K, K-1]}{g[-K, -K+1]}. \tag{B.18}$$

Similarly, letting $f[n_1, n_2] = f[-n_1, -n_2]$ given by (B.13) for $n_1 = K+1, \cdots, 2K$, $n_2 = 0, \cdots, 2K$, and $n_1 = K$, $n_2 = K, \cdots, 2K$, one can end up with

$$|g[n_1, n_2]| = |g[-n_1, -n_2]|, \qquad \forall\, [n_1, n_2] \in \Omega[K, K] \tag{B.19}$$

and

$$\frac{g[n_1, n_2]}{g[-n_1, -n_2]} = \frac{g[0, 0]}{g[0, 0]} = 1, \qquad \forall\, [n_1, n_2] \in \Omega[K, K] \tag{B.20}$$

for odd $p + q$. Therefore, $g[n_1, n_2] = g[-n_1, -n_2]$, $\forall\, [n_1, n_2] \in \Omega[K, K]$ for odd $p + q$.

Thus, we have completed the proof for P2) provided that the two assumptions B1) and B2) are true. However, the two assumptions can be relaxed by letting $K \to \infty$.

REFERENCES

[1] S. M. Kay, *Modern Spectral Estimation*. Englewood Cliffs, NJ: Prentice-Hall, 1988.

[2] D. E. Dudgeon and R. M. Mersereau, *Multidimensional Digital Signal Processing*. Englewood Cliffs, NJ: Prentice-Hall, 1984.

[3] S. R. Parker and A. H. Kayran, "Lattice parameter autoregressive modeling of two-dimensional fields–Part I: The quarter-plane case," *IEEE Trans. Acoust., Speech, Signal Processing*, vol. ASSP-32, pp. 872–885, Aug. 1984.

[4] R. L. Kashyap, R. Chellappa, and A. Khotanzad, "Texture classification using features derived from random field models," *Pattern Recognit. Lett.*, vol. 1, no. 1, pp. 43–50, 1982.

[5] R. L. Kashyap and R. Chellappa, "Estimation and choice of neighbors in spatial-interaction models of images," *IEEE Trans. Inform. Theory*, vol. IT-29, pp. 58–72, Jan. 1983.

[6] R. Chellappa and S. Chatterjee, "Classification of texture using Gaussian Markov random fields," *IEEE Trans. Acoust, Speech, Signal Processing*, vol. ASSP-33, pp. 959–963, July 1985.
[7] G. Sharma and R. Chellappa, "Two-dimensional spectrum estimation using noncausal autoregressive models," *IEEE Trans. Inform. Theory*, vol. IT-32, pp. 268–275, Feb. 1986.
[8] A. M. Tekalp, H. Kaufman, and J. E. Woods, "Identification of image and blur parameters for the restoration of noncausal blurs," *IEEE Trans. Acoust, Speech, Signal Processing*, vol. ASSP-34, pp. 963–972, July 1986.
[9] K. B. Eom, "2-D moving average models for texture synthesis and analysis," *IEEE Trans. Image Processing*, vol. 7, pp. 1741–1746, Dec. 1998.
[10] C. L. Nikias and A. P. Petropulu, *Higher-Order Spectra Analysis: A Nonlinear Signal Processing Framework*. Englewood Cliffs: Prentice-Hall, 1993.
[11] S. Bhattacharya, N. C. Ray, and S. Sinha, "2-D signal modeling and reconstruction using third-order cumulants," *Signal Process.*, vol. 62, pp. 61–72, 1997.
[12] A. Swami, G. B. Giannakis, and J. M. Mendel, "Linear modeling of multidimensional non-Gaussian processes using cumulants," *Multidimen. Syst. Signal Process.*, vol. 1, pp. 11–37, 1990.
[13] J. K. Tugnait, "Estimation of linear parametric models of nonGaussian discrete random fields with application to texture synthesis," *IEEE Trans. Image Processing*, vol. 3, pp. 109–127, Apr. 1994.
[14] T. E. Hall and G. B. Giannakis, "Image modeling using inverse filtering criteria with application to textures," *IEEE Trans. Image Processing*, vol. 5, pp. 938–949, June 1996.
[15] ——, "Bispectral analysis and model validation of texture images," *IEEE Trans. Image Processing*, vol. 4, pp. 996–1009, July 1995.
[16] M. K. Tsatsanis and G. B. Giannakis, "Object and texture classification using higher order statistics," *IEEE Trans. Pattern Anal. Machine Intell.*, vol. 14, pp. 733–750, July 1992.
[17] O. Shalvi and E. Weinstein, "Universal methods for blind deconvolution," in *Blind Deconvolution*, S. Haykin, Ed. Englewood Cliffs, NJ: Prentice-Hall, 1994.
[18] ——, "New criteria for blind deconvolution of nonminimum-phase systems (channels)," *IEEE Trans. Inform. Theory*, vol. 36, pp. 312–321, Mar. 1990.
[19] C.-C. Feng and C.-Y. Chi, "Performance of cumulant based inverse filters for blind deconvolution," *IEEE Trans. Signal Processing*, vol. 47, pp. 1922–1935, July 1999.
[20] ——, "Performance of Shalvi and Weinstein's deocnovlution criteria for channels with/without zeros on the unit circle," *IEEE Trans. Signal Processing*, vol. 48, pp. 571–575, Feb. 2000.
[21] C.-C. Feng, "Studies on cumulant based inverse filter criteria for blind deconvolution," Ph.D. dissertation, Dept. Elect. Eng., National Tsing Hua Univ., Hsinchu, Taiwan, R.O.C., June 1999.
[22] C.-Y. Chi and C.-C. Feng, "Blind channel estimation and MMSE equalization using Shalvi and Weinstein's blind deconvolution criteria," in *Proc. IEEE Wireless Commun. Networking Conf.*, New Orleans, LA, Sept. 21–24, 1999, pp. 659–663.
[23] O. Shalvi and E. Weinstein, "Super-exponential methods for blind deconvolution," *IEEE Trans. Inform. Theory*, vol. 39, pp. 504–519, Mar. 1993.
[24] M. H. Hayes, *Statistical Digital Signal Processing and Modeling*. New York: Wiley, 1996.
[25] D. M. Burley, *Studies in Optimization*. New York: Falsted, 1974.
[26] H.-M. Chien, H.-L. Yang, and C.-Y. Chi, "Parametric cumulant based phase estimation of 1-D and 2-D nonminimum phase systems by allpass filtering," *IEEE Trans. Signal Processing*, vol. 45, pp. 1742–1762, July 1997.
[27] G. Jacovitti, A. Neri, and G. Scarano, "Texture synthesis-by-analysis with hard-limited Gaussian processes," *IEEE Trans. Image Processing*, vol. 7, pp. 1615–1621, Nov. 1998.

Chong-Yung Chi (S'83–M'83–SM'89) was born in Taiwan, R.O.C., on August 7, 1952. He received the B.S. degree from the Tatung Institute of Technology, Taipei, Taiwan, in 1975, the M.S. degree from the National Taiwan University (NTU), Taipei, in 1977, and the Ph.D. degree from the University of Southern California, Los Angeles, in 1983, all in electrical engineering.

From July 1983 to September 1988, he was with the Jet Propulsion Laboratory, Pasadena, CA, where he worked on the design of various spaceborne radar remote sensing systems including radar scatterometers, synthetic aperture radars, altimeters, and rain mapping radars. From October 1988 to July 1989, he was a Visiting Specialist with the Department of Electrical Engineering at NTU. Since August 1989, he has been a Professor with the Department of Electrical Engineering, National Tsing Hua University, Hsinchu, Taiwan. He has published more than 90 technical papers in radar remote sensing, system identification and estimation theory, deconvolution and channel equalization, digital filter design, spectral estimation, and higher order statistics (HOS)-based signal processing. His research interests include signal processing for wireless communications, statistical signal processing, and digital signal processing and their applications. He has been a reviewer for the journals *Signal Processing* and *Electronics Letters*

Dr. Chi has served as a reviewer for the IEEE TRANSACTIONS ON SIGNAL PROCESSING, the IEEE TRANSACTIONS ON CIRCUITS AND SYSTEMS, and the IEEE TRANSACTIONS ON GEOSCIENCE AND REMOTE SENSING. He is an Active Member of Society of Exploration Geophysicists, a Member of European Association for Signal Processing, and an Active Member of the Chinese Institute of Electrical Engineering. He was a Technical Committee Member of both the 1997 and 1999 IEEE Signal Processing Workshops on Higher-Order Statistics (HOS) and is a Technical Committee Member of the 2001 IEEE Workshop on Statistical Signal Processing (SSP). He is also a Member of International Advisory Committee of TENCON 2001. He is a Co-Organizer and Co-chair of the 2001 IEEE SP Workshop on Signal Processing Advances in Wireless Communications (SPAWC-2001).

Chii-Horng Chen was born in Taiwan, R.O.C., on December 2, 1970. He received the B.S. degree from the Department of Control Engineering, National Chiao Tung University, Hsinchu, Taiwan, in 1992. He is currently pursuing the Ph.D. degree at National Tsing Hua University, Hsinchu.

His research interests include statistical signal processing, digital signal processing, and wireless communications.